THE JOURNAL OF PHYSICAL CHEMISTRY B
A JOURNAL OF THE AMERICAN CHEMICAL SOCIETY

pubs.acs.org/JPCB

Article

Structural Models of the First Molecular Events in the Heliorhodopsin Photocycle

Kithmini Wijesiri and José A. Gascón*

Cite This: J. Phys. Chem. B 2024, 128, 5966−5972

Read Online

ACCESS | Metrics & More | Article Recommendations | Supporting Information

ABSTRACT: Retinylidene conformations and rearrangements of the hydrogen-bond network in the vicinity of the protonated Schiff base (PSB) play a key role in the proton transfer process in the Heliorhodopsin photocycle. Photoisomerization of the retinylidene chromophore and the formation of photoproducts corresponding to the early intermediates were modeled using a combination of molecular dynamics simulations and quantum mechanical/molecular mechanics calculations. The resulting structures were refined, and the respective excitation energies were calculated. Aided by metadynamics simulations, we constructed a photoisomerized intermediate where the 13-*cis* retinylidene chromophore is rotated about a parallel pair of double bonds at C13=C14 and C15=N_Z double bonds. We demonstrate how the deprotonation of the Schiff base and the concomitant protonation of the Glu107 counterion are only favored because of these rearrangements.

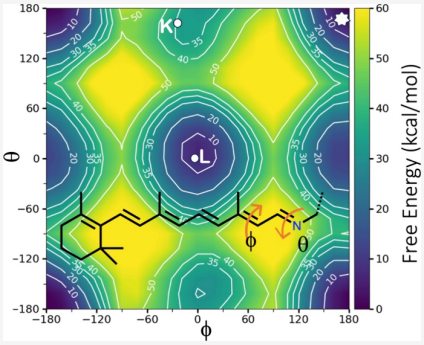

INTRODUCTION

Chromophores within light-absorbing proteins are integral to a diverse array of biological functions. The functionality of these proteins relies on the modulation of spectroscopic properties through protein−chromophore interactions. Photoreceptors belonging to the rhodopsin family comprise two key components: an apoprotein, known as opsin, and a retinylidene chromophore (RET) covalently bound to the apoprotein via a protonated Schiff base (PSB) linkage to a special lysine residue. Rhodopsins represent a broad category of membrane proteins and are distributed widely across various species, ranging from ancient protobacteria to vertebrates. Rhodopsin proteins are divided into two families, type-I microbial rhodopsins and type-II animal rhodopsins. Generally, the Schiff base is protonated, which tunes the chromophore absorption into the visible region. In certain microbial rhodopsins, such as outward H^+-pumping bacteriorhodopsins, stabilization of this positive charge is facilitated by two negatively charged counterions, namely, Asp85 and Asp212. Animal rhodopsins usually accommodate a single counterion. For example, Glu113 is highly conserved in vertebrate visual and nonvisual opsins.[1]

In 2018, a new family of rhodopsins named Heliorhodopsins (HeRs) was discovered using functional metagenomics.[2] HeRs are widely distributed among bacteria, archaea, algae, and algal viruses. They are distinct from the type-I and type-II rhodopsins (<15% in sequence identity)[3] and exhibit unique features, including an opposite orientation in the membrane and longer photocycles. HeR's extracellular part is completely hydrophobic.[4] HeRs possess a single counterion of the Schiff base, similar to the inward H^+-pumping microbial rhodopsins (xenorhodopsin and schizorhodopsin), anion-channel rhodopsins, and the type-II rhodopsins.[1] In HeR-48C12, the Schiff base linkage with the all-*trans* RET chromophore is formed via Lys241 in the G-helix, and Glu107 in the C-helix serves as the counterion to the PSB (Figure 1).

The photoactivation mechanism of Heliorhodopsin is still not well understood. Previous studies have suggested that HeR-48C12 does not function as an ion transporter or channel.[2] Similarities with sensory rhodopsin I and II in the length of the photocycle (larger than 1 s) suggest that HeRs act as light-activated sensors.[5] HeRs are predominantly confined to the upper layer of aquatic environments that receives sufficient sunlight for photosynthesis, indicating their possible role in light-harvesting.[2] Consequently, there is considerable interest in decoding their photoactivation at the molecular level. A logical initial approach is to compare their photocycles with that of bacteriorhodopsin. In bacteriorhodopsin (bR), the chromophore undergoes a light-induced isomerization, transitioning from the all-*trans* to the 13-*cis* configuration. This change initiates a proton transfer from the Schiff base to its counterion. Subsequent dynamical changes within the protein generate a proton-pumping process that contributes to the generation of a proton gradient, which is ultimately utilized for ATP synthesis. Each intermediary state

Received: February 5, 2024
Revised: May 29, 2024
Accepted: June 5, 2024
Published: June 14, 2024

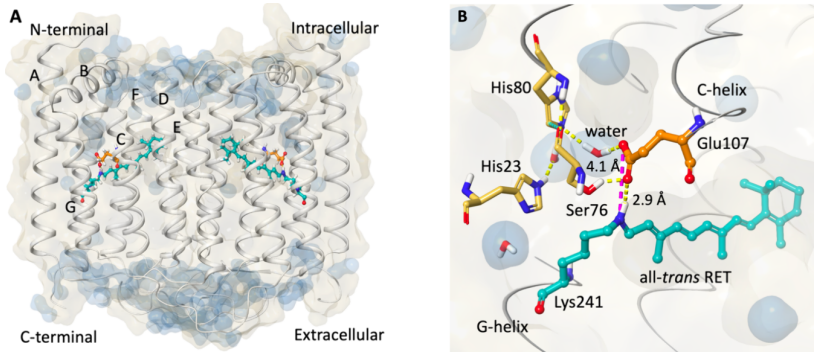

Figure 1. (A) Dimeric form of the dark state HeR-48C12 (PDB code: 6SU3). The all-*trans* RET (teal) forms a protonated Schiff base (PSB) linkage with the G-helix. Protein counterion (orange) consists of Glu107 on the C-helix. (B) Close up view of the PSB and its immediate environment. The retinylidene chromophore is covalently bound to the amino group of Lys241. The yellow and purple dashed lines represent a hydrogen bond and a salt bridge, respectively. In (B), the front helices have been omitted for clarity.

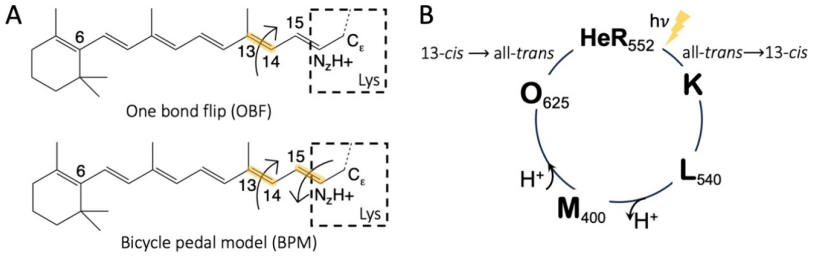

Figure 2. (A) RET photoisomerization of HeR via one-bond flip and bicycle-pedal isomerization mechanisms. (B) Model of the HeR-48C12 photocycle. Photointermediates are named alphabetically from K to O, starting with the dark state indicated as HeR. The maximum absorption wavelength (in nm) of the different intermediates is indicated as a lowercase number for the states were these values are reported.[2,12,13] The sequential steps of the H^+ transport (RET deprotonation and protonation) are indicated at the respective photointermediate transitions as shown in the work of Pushkarev et al.[2]

within the photocycle has been characterized by unique spectroscopic and functional properties.[6]

The classical one-bond flip (OBF) around the C13=C14 double bond, which requires a significant displacement of the PSB (Figure 2A), represents the simplest mechanism for generating a nonrestricted isomerization.[7] In reality, such a motion is largely inhibited by the covalently bound lysine residue that forms the PSB. In 1976, in a seminal study of the vision process in vertebrate rhodopsin, Warshel proposed a concerted rotation about parallel pairs of double bonds, what he called the "bicycle-pedal (BP) model".[8] Warshel later revised the model to one in which the isomerization motion involves partial rotation around several bonds, in addition to the main parallel pairs of bonds.[9] More recently, computational work by Olivucci and co-workers showed that the first event in the photoactivation mechanism in both bR and TaHer (a Heliorhodopsin) is better described as an aborted bicycle-pedal motion.[10,11]

Absorption spectra of natural variants of Heliorhodopsins from various microorganisms have been measured using UV−visible spectroscopy. The absorption maximum wavelength (λ_{max}) is in the range of 530−556 nm. The wild-type HeR-48C12 shows an absorption maximum of 552 nm.[3] Upon absorbing a photon, the RET chromophore in HeR-48C12 undergoes isomerization, initiating a cascade of conformational changes through a series of metastable intermediates. These intermediates are characterized by their functional role and spectral features throughout the photocycle (Figure 2B). These intermediates have been named following the nomenclature used in the bacteriorhodopsin photocycle (i.e., formation of K, L, M, and O photointermediates).[2] While there are no structural reports of any these intermediates in HeR, certain conformational changes have been inferred via FTIR and time-resolved resonance Raman spectroscopy.[2] Time-resolved resonance Raman spectroscopy provided evidence for the existence of the L intermediate,[12] distinguished by its absorption peak at approximately 540 nm.[2] It was suggested that the PSB's hydrogen bond is weakened in the K intermediate. On the other hand, the spectrum of the L intermediate exhibited a larger deuteration shift compared to the K state, indicating the reformation of the hydrogen bond with the PSB, priming the system for proton transfer.

The M intermediate, with an absorption maxima of ∼400 nm,[2] corresponds to a deprotonated Schiff base, which accompanies protonation of the counterion in many type-I rhodopsins. From M to O, a proton returns to the Schiff base. The O intermediate is characterized by a red-shifted absorption maximum of ∼625 nm.[2] The longer absorption wavelength observed in the O state could be directly linked to alterations in the electrostatic environment such as proton uptake in the O state and shifts in protonation or polarization within protein sorroundings.[14] In contrast to the K and M intermediates, the O intermediate exhibited significant alterations in amide-I vibrations, suggesting extensive conformational changes.[2] Ultimately, the protein reverts to its dark state through thermal isomerization.

The early intermediates in the bR photocycle have been determined by cryoelectronic microscopy and X-ray crystallog-

https://doi.org/10.1021/acs.jpcb.4c00804
J. Phys. Chem. B 2024, 128, 5966−5972

raphy.[15,16] However, structural data on HeRs is limited to the very recently reported ground-state crystallographic structures of actinobacterial HeR-48C12 (PDB: 6SU3 at pH 8.8, 6SU4 at pH 4.3)[4] and archaeal TaHeR (PDB: 6IS6, 7U55 at pH 4.5 and E108D mutant 7CLJ).[17,18] To the best of our knowledge, X-ray crystallographic structures of HeR intermediate states have not been reported. Thus, the goal of this present work is to simulate the molecular changes along the photocycle in HeR and make a connection between structural changes and the reported spectroscopy, focusing on the changes occurring from the dark state to the M state. Due to the high similarity with the bR photocycle, in terms of the spectroscopy of the intermediates, we use bR's structures as reference and validation. We develop an approach using metadynamics to create models of the K, L, and M states via ground-state simulations. With these models, we are able to rationalize the energetics of proton transfer from the PSB to its counterion.

COMPUTATIONAL APPROACH

To study the early stages of the HeR-48C12 photocycle, we performed a series of MD simulations and combined QM/MM calculations. All calculations are based on the highest resolution X-ray structure available for HeR-48C12 (PDB: 6SU3, resolution 1.50 Å) in the violet form solved at pH 8.8. The crystal structure with the two monomers was used since dimerization plays a key role in the overall folding and stability of HeR.[7] The protein preparation application within Maestro (Schrödinger Release 2022-1) was used to preprocess the complex, assigning bond orders, adding hydrogens, and filling in missing loops. For the alternative side chain positions reported in the crystal structures, the most populated ones were kept according to their PDB β-factor. Optimization of hydrogen-bond assignment was performed at pH 8.8. Crystallographic waters near the Schiff base were kept since they play an important role in the formation of an extended hydrogen-bonded network for proton transfer.[19] All other molecules (OLC, LFA, OLA, and GOL) in the X-ray structure were deleted. A preliminary restrained minimization was applied for hydrogens only. Subsequently, the protein dimer was embedded in a predefined POPC (1-palmitoyl-2-oleoyl-*sn*-glycero-3-phosphatidylcholine) membrane. The area per lipid is approximately 85 Å^2. An orthorhombic box was constructed using the TIP3P water model by creating a 10 Å buffer from the protein. The PROPKA method,[21] within the protein preparation software, was used to refine the protonation states and tautomerization of all amino acids at pH 8.8. To ensure that the system maintains overall electrical neutrality, Cl^- ions were added to neutralize the system. A NaCl salt concentration of 0.15 M was also added to the system. The system in its entirety contained approximately 51,000 atoms. The OPLS4 force field[20] was used for all preliminary minimizations and MD simulations. OPLS4, which is derived from the original OPLS force field, incorporates an extended torsional parametrization along with refined partial charge assignment. The force field assignment algorithm within Schrodinger differentiates single and double bonds in the retinal's polyene chain, even though all carbon atoms are sp2. Figure S5 and Table S6 show the bond lengths, typical coordinates of the ret-lys system, and the force field charges. All MD simulations were run on Nvidia GPU hardware with Desmond (Schrödinger 2022-1). A relaxation protocol was performed (detailed in the Supporting Information under MD Methods) prior to the production MD. Subsequently, simulations were conducted over a total duration of 200 ns using the NPT ensemble (300 K, 1 atm). MD simulations were carried out for the dark-adapted state and other intermediates generated via metadynamics simulations (*vide infra*). Additional information about the molecular dynamics analysis, including root-mean-square deviation (RMSD) calculations, is reported in the Supporting Information. Snapshots were extracted every 5 ns interval to perform statistics and additional QM/MM calculations.

Metadynamics. Well-tempered metadynamics (WT-metaD)[21] were performed starting from the dark state structure to produce a path to create the isomerized state following a bicycle-pedal model. The collective variables (CVs) were defined as the dihedral angles C12-C13-C14-C15 (CV1) and C14-C15-N_z-C_e (CV2). The width of the Gaussian potential was w = 5.0, and the initial height h_0 = 0.1 kcal mol^{-1}. The deposition time was Δt = 0.1 ps, and the bias factor of WT-metaD ($k_B\Delta T$) was set to 20 kcal/mol. The ensemble class and relaxation protocol were like those employed in the equilibrium MD. It is important to emphasize that the goal of the WT-metaD simulations is to simply steer the chromophore throughout the different intermediates. We made no attempt to simulate the actual nonadiabatic dynamics on the excited state. Thus, the path of isomerization follows a hypothetical thermal process in the dark. Nonetheless, local minima in this path should correspond to the experimental characterization. It is worth mentioning that thermal isomerization has a biological importance of its own, which has been shown to control thermal noise in the photoisomerization of visual rhodopsins.[22,23]

Structure Optimizations and Electronic Structure Calculations. Hybrid QM/MM calculations were run on 200 snapshots extracted from different stages of the MD and WT-metaD. The QM/MM boundary was placed between the C_γ and C_β of Lys241 and between C_β and C_α of Glu107 using the hydrogen link method. Thus, the QM part contains RET, part of Lys241's side chain and Glu107's side chain. The OPLS4 force field was used to treat the rest of the protein, POPC membrane and the solvent system at the MM level. We describe the chromophore fluctuations at finite temperature using an approach that we recently introduced in the study of spectral properties of carotenoid proteins, where the QM region alone is optimized at the QM/MM level.[24,25] This refinement aims to better describe the bond length alternation (BLA) of the chromophore, which is largely overestimated by conventional force fields. These local optimizations were performed at the DFT B3LYP/6-31G* level using QSite (Schrödinger 2022-1). All QM/MM calculations use electrostatic embedding. The B3LYP/6-31G* level of theory has proven very reliable to obtain accurate geometries in retinal molecules and other isoprenoid-based molecules such as carotenoids.[26−28] To calculate the absorption maxima and spectral shifts of preferred intermediate states, single-point excited-state energies were carried out on the optimized structures via TDDFT with SVWN/6-31G*. We have chosen the SVWN functional as it best reproduces the excitation energy measured and calculated by Rajput et al.[29] and our previous study on HeR absorption shifts.[30]

For the L to M step, which involves proton transfer from the PSB to Glu107, we estimated the proton transfer energy barriers following the adiabatic mapping approach developed for enzymatic reactions.[31,32] This approach requires the definition of a coordinate to model the reaction, which in our case, is the H−O bond length in the N−H···O salt bridge.

https://doi.org/10.1021/acs.jpcb.4c00804
J. Phys. Chem. B 2024, 128, 5966−5972

Then, snapshots from an MD simulation are used to optimize the QM/MM system at fixed reaction coordinates, progressing from reactants to products. The maximum value of the QM/MM energy along that path is then averaged over those snapshots (50 in our case). Using the computed energy barriers, we estimated the thermal rate constant, taking into account tunneling effects, using the variational transition state theory[33] (VTST) implemented in the kSC.py program by Serra-Peralta et al.[34] In brief, VTST is a semiclassical theory that corrects the classical rate constant $k_c(T)$ by including the tunneling rate constant $k_t(T)$: $k_{SC} = k_t(T)\ k_c(T)$, where $k_c(T)$ is given by the Eyring's transition state theory. Details on the evaluation of k_{SC} were developed by Bao and Truhlar.[33] The VTST, implemented by Serra-Peralta,[34] is a unidimensional approach, which requires a potential curve interpolation between the reactant and products. In our case, we used the asymmetric Eckart interpolation.

RESULTS

Model of the Photoisomerized State. To produce a model of the photoisomerized state and subsequent intermediates, we performed a 2D metadynamics simulation with the collective variables defined above. Figure 3 shows the free energy surface (FES) as a function of these two collective variables. Based on the FES, conformations with local free energy minima occur at various combinations of (CV1, CV2). The state (180°, 180°) corresponds, nominally, to the dark-adapted state (all-*trans* RET model). The end state that follows a double isomerization corresponds to the (0°, 0°) combination. Note that the path from (180°, 180°) to (0°, 0°) does not necessarily follow a minimum energy path (MEP) on the ground-state free-energy landscape since the actual path is a result of a nonadiabatic excited-state process. Thus, while one would be tempted to draw an MEP from (180°, 180°) → (180°, 0°) → (0°, 0°), crystallographic[16,35−40] and theoretical[10] models of bR have shown that the first intermediate (K state) corresponds to configurations near the (0°, 180°) basin.[37] While there is no consensus on the precise structure of the K state (scattered symbols in Figure 3), most of the models point to a state characterized by CV1 < 0° and CV2 < 180°. The median values from these studies are around (−28°, 155°). Based on these observations, we optimized all the metadynamic snapshots in the region −40° < CV1 < 40° and 120° < CV2 < 180° at the QM/MM level. We obtained median values of (−19.9°, 159°), which is in good agreement with the median of these previous studies. Thus, in the discussion that follows, we assign the K state to configurations near (−19.9°, 159°). We further justify this assignment in the next section by comparing typical snapshots in this vicinity with one of the crystallographic models of the K state in bR. We will also show that the (0°, 0°) configuration promotes proton transfer from the PSB to the counterion. Thus, we assign the L state to this configuration.

Having identified the energy basins in the free energy surface for the dark, K, and L states, we performed equilibrium MD simulations starting from representative snapshots of these energy basins. Representative snapshots of these equilibrium MDs are shown in Figure 4. For the M state, we took a snapshot of the L-state MD simulation and placed the proton of the PSB on the nearest carboxylate oxygen atom of Glu107. Below, we analyze in more detail these four states.

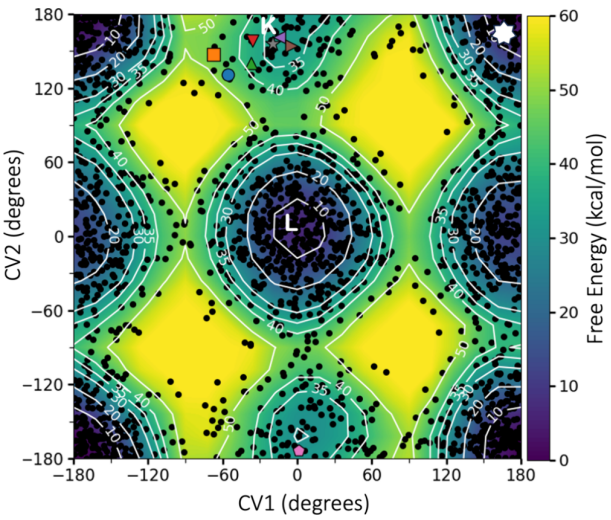

Figure 3. Free-energy profile obtained from the metadynamics simulation. (CV1, CV2) are defined as the dihedrals CV1 = C12-C13-C14-C15 and CV2 = C14-C15-N_z-C_ε. The dark-adapted all-*trans* state (white star) corresponds, nominally, to the configuration (180°, 180°). The K and L states correspond to configurations in the vicinity of (180°, 0°), and (0°, 0°), respectively. The small dark circles reflect the density of points visited by the metadynamics simulation. The colored symbols correspond to various experimental and computational assignments of the K state for bacteriorhodopsin. (blue circle) Schobert et al.;[35] (orange square) Nass Kovacs et al.;[36] (green triangle) Taguchi et al.;[37] (red inverted triangle) Nogly et al.;[38] (violet left-pointing triangle) Borshchevskiy et al.;[39] (olive-green right-pointing triangle) Matsui et al.;[40] (pink pentagon) Edman et al.;[16] (gray star) Altoè et al.[10] (computational).

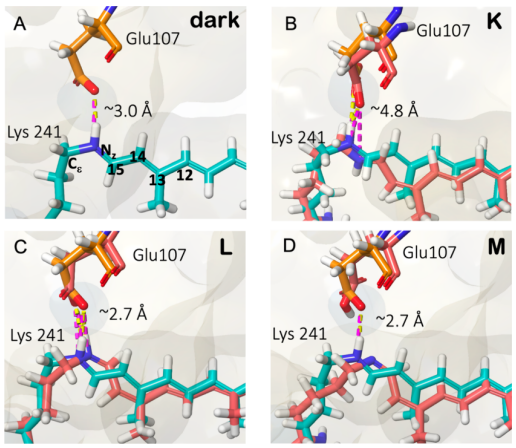

Figure 4. (A−C) Typical snapshots along equilibrium MD simulations whose starting geometries are taken from the free-energy basins in Figure 3. These three snapshots represent the dark, K, and L states, respectively. (D) Representative snapshot of an equilibrium MD simulation where the proton is placed in Glu107 starting from an L-state snapshot. Thus, D represents the M state. In the dark state, the PSB is stabilized with a H-bond and a salt bridge with Glu107. In the K state, a one-bond isomerization causes the Schiff base to lose its H-bond. In the L state, an additional isomerization causes the H-bond to reform, gaining 0.3 Å in the PSB−counterion distance. In the M state, the Schiff base transfers its proton to Glu 107. Intermediate states are superimposed with the ground-state RET for comparison. The all-*trans* and intermediate models are shown in teal and faded red, respectively.

https://doi.org/10.1021/acs.jpcb.4c00804
J. Phys. Chem. B 2024, 128, 5966−5972

Structural Models of K, L, and M Intermediates. *Dark → K.* In the dark state (Figure 4A), the N_z of the PSB makes a H-bond with Glu107. Resonance Raman and FTIR spectra indicate that the RET is in a twisted 13-*cis* configuration in the K state of the bR.[41] This observation was later confirmed by producing crystallographic models via low-temperature trapping of intermediates.[16,35−40] As shown in the previous section, we were able to obtain an HeR intermediate like that of bR's K state through our metadynamics simulations. Our K state is generally in good agreement with previous crystallographic models for bR. In particular, our model most closely resembles the structure of Borshchevskiy et al.[39] (PDB code: 7Z0C, Figure S5).

In the K intermediate, the Schiff base reorients and removes the H-bond formed between the PSB and the negatively charged carboxylate of Glu107 (Figure 4B). The reorientation of the NH+ bond produces a charge separation state with an energy difference of ∼32 kcal/mol with respect to the all-*trans* state. This energy difference is in the range of the energy storage measured for vertebrate rhodopsins (32−24 kcal/mol)[42,43] and confirms early QM/MM models on the mechanism of energy storage that pointed out that such a large energy difference must come from electrostatic interactions.[44]

L → M. The conformation at the L state in the photocycle is of particular importance as the active site is now primed for deprotonation. According to Pushkarev et al., a proton transfer event occurs during the L-state to M-state transition on a time scale of ∼5 μs.[2] In this step, a proton is transferred from the PSB to a proton-accepting group, likely composed of several amino acid residues, including His23 and His80.[2] It is logical to assume that the first step in the L to M transition is the proton transfer from PSB to Glu107.

To characterize the energetics of Schiff base deprotonation, we took 200 snapshots from this equilibrium MD of the K state and locally optimize these snapshots at the QM/MM level following the protocol described in the methods section. The average QM/MM energy over those snapshots was then collected. From these minimized snapshots, we manually transferred the proton to the closest oxygen atom of Glu107. Again, these snapshots were locally optimized at the QM/MM level energy and their average energy was collected. The difference between these two averages defines the proton transfer reaction energy for the L → M step. We also performed the same exact procedure but using the equilibrium MD of the dark-adapted all-*trans* state. The energetics of proton transfer are presented in Table 1. As detailed in the methods section, we also computed the reaction barrier for the two states using the adiabatic mapping method. Table 1 clearly shows that proton transfer is highly favored in the L state, as compared to the dark state.

While in neither case we would expect an equilibrium population of a protonated Glu107, the proton transfer rate is 3 orders of magnitude faster in the L state. This feature coupled with other rearrangements known to occur in the M state would kinetically allow the proton to later transfer to the proton-accepting group (PAG). The most likely next step, within the M state, is the transfer of the proton from Glu107 to the His80/His23 moiety, as proposed by Pushkarev et al.[2]

A recent MD-based QM/MM study that also focused on the conformational changes that accompany proton transfer from L to M and the subsequent changes toward the O state is also worth noting.[45] However, in such study, the dark all-*trans* state was used as a model of the L state. Thus, their energetics are roughly comparable to our proton transfer analysis in the dark state (first row of Table 1). While they find a transfer energy of ∼12 kcal/mol, we obtain, via the adiabatic mapping approach, 7.2 kcal/mol. Moreover, we additionally show that the distortions, which drive the conversion from dark to K to L, lower this reaction energy to 4.3 kcal/mol.

Spectrum of Early Intermediates. As shown above, the RET chromophore undergoes conformational changes during the formation of early intermediates, resulting in significant H-bond network rearrangements in the RET binding pocket. We decomposed and analyzed the QM/MM energies of these intermediate structures to see if we could reproduce the absorption maxima and assign the molecular models to their respective intermediate states. The vertical excitation energies (λ_{max}) and oscillator strengths (f) of the intermediate states were calculated via DFT SVWN/6-31G*, and the calculated results were compared with the experimental values in Table 2.

Absorbance of the all-*trans* state (536 nm) is consistent with measurements of the absorption spectrum of Heliorhodopsin (552 nm). As established through studies of a number of RET salts,[46] the distance between the PSB and the counterion has the largest effect on the spectral shift. Stronger or weaker electrostatic interactions with the counterion cause a spectral blue-or red-shift, respectively.[18] The distance from PSB to the counterion increases to ∼4.8 Å in the K-state. The weakening of the interactions between retinal and its counterion, mainly due to the breaking of the N−H hydrogen bond (Figure 4B), causes a red shift in the absorbance compared to the dark state. Even though the absorbance maximum of HeR K-state is not reported, this is in accordance with other microbial rhodopsins which exhibits slight red-shifted absorbances for the K-state.[16,47] The interaction between the chromophore and its counterion is restored and strengthened in the L-state as a result of the bicycle-pedal rotation, which brings the retinal and its counterion 2.7 Å apart (Figure 4C). Literature reports a 12 nm blue shift for the L-state compared to ground state as seen in Table 2. We observe a ∼ 6 nm blue shift for the L-state from our QM calculations. The primary proton transfer event from the Schiff base to the proton accepting group induces a blue shift in the M-state. This considerably large blue shift in the M-state with respect to the L-state is clearly due to the deprotonation of the RET Schiff base. Our calculations show a ∼ 82 nm blue shift which is in quantitative agreement with the literature. Therefore, we were able to successfully reproduce the ground state absorbance maxima, a slight red shift in the K-intermediate, and the expected blue shifts in the L- and M-intermediates.

Table 1. Comparison of the Energetics of the Proton Transfer Reaction from the PSB to Glu107 for Both the Dark and L States

	reaction energy	reaction barrier	tunneling rate constant at 300 K
dark state	7.2 ± 0.3 kcal/mol	8.9 ± 0.6 kcal/mol	6.5×10^6 s^{-1}
L	4.3 ± 0.3 kcal/mol	5.9 ± 0.4 kcal/mol	4.9×10^9 s^{-1}

CONCLUSIONS

In the present study we performed molecular dynamics, metadynamics and hybrid QM/MM calculations to examine the conformational changes of HeR after the *trans-cis*

https://doi.org/10.1021/acs.jpcb.4c00804
J. Phys. Chem. B 2024, 128, 5966−5972

Table 2. Single-Point QM Calculations (SVWN/6-31G*) of λ_{max} and Oscillatory Strengths (f) on Optimized Structures at the B3LYP/6-31G* Level Taken from MD Simulations of HeR-48C12 PSB All-*Trans* and Other Intermediates[a]

				Experimental λ_{max} /nm	
State	Calc. λ_{max} (nm)	Confidence Interval (nm)	f	Heliorhodopsin	Bacteriorhodopsin[16]
all-*trans*-PSB	536.0	1.6	1.3	552[3]	570
K-state	541.1	2.0	1.3	N/A	590
L-state	530.9	1.6	1.0	540[2]	550
M-state	454.3	1.3	1.3	400[2]	412

[a]Results are expressed as the mean of 200 snapshots. Standard deviation of λ_{max}, f, and 95% confidence intervals are presented in the Supporting Information (Table S5). Experimental λ_{max} values are also reported for HeR and bR.

photoisomerization of the RET chromophore via a double isomerization motion. This motion is achieved over the ground state energy surface. On this surface, a model of the K-state is proposed in which the hydrogen bond between the Schiff base and its counterion Glu107 breaks. Further rotation of the adjacent double bond reconnects the Schiff base with its counterion, thus defining the L-state. This reconnection strengthens their hydrogen bond and primes the active site for proton transfer. Calculations showed that the L intermediate has faster proton transfer kinetics from the Schiff base to Glu107 compared to the dark state, consistent with observations. Overall, the computations reveal how retinal rearrangements in early photocycle intermediates promote Schiff base deprotonation and subsequent proton transfer steps in HeRs and how these conformational changes tune the absorption spectrum.

■ ASSOCIATED CONTENT

Supporting Information

The Supporting Information is available free of charge at https://pubs.acs.org/doi/10.1021/acs.jpcb.4c00804.

Additional details of the MD simulations. MD RMSD analysis. Comparison of the HeR K-state model and the crystal structure of bR K-state. N−O distance in all-*trans* and L-state models. Energetics of proton transfer for all-*trans* and L-state HeR. QM calculations on optimized models from MD simulations of all-*trans*, K-state, L-state and M-state. Coordinates and Force field charges of the Ret-Lys system (PDF)

■ AUTHOR INFORMATION

Corresponding Author

José A. Gascón − *Department of Chemistry, University of Connecticut, Storrs, Connecticut 06269-3060, United States;* orcid.org/0000-0002-4176-9030; Email: jose.gascon@uconn.edu

Author

Kithmini Wijesiri − *Department of Chemistry, University of Connecticut, Storrs, Connecticut 06269-3060, United States*

Complete contact information is available at: https://pubs.acs.org/10.1021/acs.jpcb.4c00804

Notes

The authors declare no competing financial interest.

■ ACKNOWLEDGMENTS

This work was supported by the National Science Foundation, Award CHE-2203567 (to J.A.G). Computational resources for this work have been provided through the University of Connecticut Storrs High Performance Computing Center.

■ REFERENCES

(1) Nagata, T.; Inoue, K. Rhodopsins at a Glance. *J. Cell. Sci.* **2021**, *134* (22), jcs258989.

(2) Pushkarev, A.; Inoue, K.; Larom, S.; Flores-Uribe, J.; Singh, M.; Konno, M.; Tomida, S.; Ito, S.; Nakamura, R.; Tsunoda, S. P.; Philosof, A.; Sharon, I.; Yutin, N.; Koonin, E. V.; Kandori, H.; Béjà, O. A Distinct Abundant Group of Microbial Rhodopsins Discovered Using Functional Metagenomics. *Nature* **2018**, *558* (7711), 595−599.

(3) Kim, S.-H.; Chuon, K.; Cho, S.-G.; Choi, A.; Meas, S.; Cho, H.-S.; Jung, K.-H. Color-Tuning of Natural Variants of Heliorhodopsin. *Sci. Rep.* **2021**, *11* (1), 854.

(4) Kovalev, K.; Volkov, D.; Astashkin, R.; Alekseev, A.; Gushchin, I.; Haro-Moreno, J. M.; Chizhov, I.; Siletsky, S.; Mamedov, M.; Rogachev, A.; Balandin, T.; Borshchevskiy, V.; Popov, A.; Bourenkov, G.; Bamberg, E.; Rodriguez-Valera, F.; Büldt, G.; Gordeliy, V. High-Resolution Structural Insights into the Heliorhodopsin Family. *Proc. Natl. Acad. Sci. U.S.A.* **2020**, *117* (8), 4131−4141.

(5) Besaw, J. E.; Reichenwallner, J.; De Guzman, P.; Tucs, A.; Kuo, A.; Morizumi, T.; Tsuda, K.; Sljoka, A.; Miller, R. J. D.; Ernst, O. P. Low pH Structure of Heliorhodopsin Reveals Chloride Binding Site and Intramolecular Signaling Pathway. *Sci. Rep.* **2022**, *12* (1), 13955.

(6) Otomo, A.; Mizuno, M.; Singh, M.; Shihoya, W.; Inoue, K.; Nureki, O.; Béjà, O.; Kandori, H.; Mizutani, Y. Resonance Raman Investigation of the Chromophore Structure of Heliorhodopsins. *J. Phys. Chem. Lett.* **2018**, *9* (22), 6431−6436.

(7) Liu, R. S. H.; Hammond, G. S. The Case of Medium-Dependent Dual Mechanisms for Photoisomerization: One-Bond-Flip and Hula-Twist. *Proc. Natl. Acad. Sci. U.S.A.* **2000**, *97* (21), 11153−11158.

(8) Warshel, A. Bicycle-Pedal Model for the First Step in the Vision Process. *Nature* **1976**, *260* (5553), 679−683.

(9) Warshel, A.; Chu, Z. T.; Hwang, J.-K. The Dynamics of the Primary Event in Rhodopsins Revisited. *Chem. Phys.* **1991**, *158* (2), 303−314.

(10) Altoè, P.; Cembran, A.; Olivucci, M.; Garavelli, M. Aborted Double Bicycle-Pedal Isomerization with Hydrogen Bond Breaking Is the Primary Event of Bacteriorhodopsin Proton Pumping. *Proc. Natl. Acad. Sci.wijesiri* **2010**, *107* (47), 20172−20177.

(11) Palombo, R.; Barneschi, L.; Pedraza-González, L.; Yang, X.; Olivucci, M. Picosecond Quantum-Classical Dynamics Reveals That the Coexistence of Light-Induced Microbial and Animal Chromophore Rotary Motion Modulates the Isomerization Quantum Yield of Heliorhodopsin. *Phys. Chem. Chem. Phys.* **2024**, *26* (13), 10343−10356.

(12) Urui, T.; Mizuno, M.; Otomo, A.; Kandori, H.; Mizutani, Y. Resonance Raman Determination of Chromophore Structures of Heliorhodopsin Photointermediates. *J. Phys. Chem. B* **2021**, *125* (26), 7155−7162.

(13) Shibukawa, A.; Kojima, K.; Nakajima, Y.; Nishimura, Y.; Yoshizawa, S.; Sudo, Y. Photochemical Characterization of a New Heliorhodopsin from the Gram-Negative Eubacterium *Bellilinea Caldifistulae* (BcHeR) and Comparison with Heliorhodopsin-48C12. *Biochemistry* **2019**, *58* (26), 2934−2943.

(14) Noji, T.; Ishikita, H. Mechanism of Absorption Wavelength Shift of Bacteriorhodopsin During Photocycle. *J. Phys. Chem. B* **2022**, *126* (48), 9945−9955.
(15) Neutze, R.; Pebay-Peyroula, E.; Edman, K.; Royant, A.; Navarro, J.; Landau, E. M. Bacteriorhodopsin: A High-Resolution Structural View of Vectorial Proton Transport. *Biochim. Biophys. Acta, Biomembranes.* **2002**, *1565* (2), 144−167.
(16) Edman, K.; Nollert, P.; Royant, A.; Belrhali, H.; Pebay-Peyroula, E.; Hajdu, J.; Neutze, R.; Landau, E. M. High-Resolution X-Ray Structure of an Early Intermediate in the Bacteriorhodopsin Photocycle. *Nature* **1999**, *401* (6755), 822−826.
(17) Shihoya, W.; Inoue, K.; Singh, M.; Konno, M.; Hososhima, S.; Yamashita, K.; Ikeda, K.; Higuchi, A.; Izume, T.; Okazaki, S.; Hashimoto, M.; Mizutori, R.; Tomida, S.; Yamauchi, Y.; Abe-Yoshizumi, R.; Katayama, K.; Tsunoda, S. P.; Shibata, M.; Furutani, Y.; Pushkarev, A.; Béjà, O.; Uchihashi, T.; Kandori, H.; Nureki, O. Crystal Structure of Heliorhodopsin. *Nature* **2019**, *574* (7776), 132−136.
(18) Tanaka, T.; Singh, M.; Shihoya, W.; Yamashita, K.; Kandori, H.; Nureki, O. Structural Basis for Unique Color Tuning Mechanism in Heliorhodopsin. *Biochem. Biophys. Res. Commun.* **2020**, *533* (3), 262−267.
(19) Bas, D. C.; Rogers, D. M.; Jensen, J. H. Very Fast Prediction and Rationalization of pKa Values for Protein-Ligand Complexes. *Proteins* **2008**, *73* (3), 765−783.
(20) Lu, C.; Wu, C.; Ghoreishi, D.; Chen, W.; Wang, L.; Damm, W.; Ross, G. A.; Dahlgren, M. K.; Russell, E.; Von Bargen, C. D.; Abel, R.; Friesner, R. A.; Harder, E. D. OPLS4: Improving Force Field Accuracy on Challenging Regimes of Chemical Space. *J. Chem. Theory Comput.* **2021**, *17* (7), 4291−4300.
(21) Barducci, A.; Bussi, G.; Parrinello, M. Well-Tempered Metadynamics: A Smoothly Converging and Tunable Free-Energy Method. *Phys. Rev. Lett.* **2008**, *100* (2), No. 020603.
(22) Luk, H. L.; Bhattacharyya, N.; Montisci, F.; Morrow, J. M.; Melaccio, F.; Wada, A.; Sheves, M.; Fanelli, F.; Chang, B. S. W.; Olivucci, M. Modulation of Thermal Noise and Spectral Sensitivity in Lake Baikal Cottoid Fish Rhodopsins. *Sci. Rep.* **2016**, *6* (1), 38425.
(23) Gozem, S.; Schapiro, I.; Ferré, N.; Olivucci, M. The Molecular Mechanism of Thermal Noise in Rod Photoreceptors. *Science* **2012**, *337* (6099), 1225−1228.
(24) Pigni, N. B.; Clark, K. L.; Beck, W. F.; Gascón, J. A. Spectral Signatures of Canthaxanthin Translocation in the Orange Carotenoid Protein. *J. Phys. Chem. B* **2020**, *124* (50), 11387−11395.
(25) Clark, K.; Pigni, N. B.; Wijesiri, K.; Gascón, J. A. Spectral Features of Canthaxanthin in HCP2. *A QM/MM Approach. Molecules* **2021**, *26* (9), 2441.
(26) Gascón, J. A.; Sproviero, E. M.; Batista, V. S. Computational Studies of the Primary Phototransduction Event in Visual Rhodopsin. *Acc. Chem. Res.* **2006**, *39* (3), 184−193.
(27) Guberman-Pfeffer, M. J.; Greco, J. A.; Birge, R. R.; Frank, H. A.; Gascón, J. A. Light Harvesting by Equally Contributing Mechanisms in a Photosynthetic Antenna Protein. *J. Phys. Chem. Lett.* **2018**, *9* (3), 563−568.
(28) Guberman-Pfeffer, M. J.; Gascón, J. A. Carotenoid-Chlorophyll Interactions in a Photosynthetic Antenna Protein: A Supramolecular QM/MM Approach. *Molecules* **2018**, *23* (10), 2589.
(29) Rajput, J.; Rahbek, D. B.; Andersen, L. H.; Hirshfeld, A.; Sheves, M.; Altoè, P.; Orlandi, G.; Garavelli, M. Probing and Modeling the Absorption of Retinal Protein Chromophores in Vacuo. *Angew. Chem., Int. Ed.* **2010**, *49* (10), 1790−1793.
(30) Wijesiri, K.; Gascón, J. A. Microsolvation Effects in the Spectral Tuning of Heliorhodopsin. *J. Phys. Chem. B* **2022**, *126* (31), 5803−5809.
(31) Ranaghan, K. E.; Mulholland, A. J. Investigations of Enzyme-Catalysed Reactions with Combined Quantum Mechanics/Molecular Mechanics (QM/MM) Methods. *Int. Rev. Phys. Chem.* **2010**, *29* (1), 65−133.
(32) Lonsdale, R.; Harvey, J. N.; Mulholland, A. J. A Practical Guide to Modelling Enzyme-Catalysed Reactions. *Chem. Soc. Rev.* **2012**, *41* (8), 3025−3038.
(33) Bao, J. L.; Truhlar, D. G. Variational Transition State Theory: Theoretical Framework and Recent Developments. *Chem. Soc. Rev.* **2017**, *46* (24), 7548−7596.
(34) Serra-Peralta, M.; Domínguez-Dalmases, C.; Rimola, A. Water Formation on Interstellar Silicates: The Role of Fe2+/H2 Interactions in the O + H2 → H2O Reaction. *Phys. Chem. Chem. Phys.* **2022**, *24* (46), 28381−28393.
(35) Schobert, B.; Cupp-Vickery, J.; Hornak, V.; Smith, S. O.; Lanyi, J. K. Crystallographic Structure of the K Intermediate of Bacteriorhodopsin: Conservation of Free Energy after Photoisomerization of the Retinal. *J. Mol. Biol.* **2002**, *321* (4), 715−726.
(36) Nass Kovacs, G.; Colletier, J.-P.; Grünbein, M. L.; Yang, Y.; Stensitzki, T.; Batyuk, A.; Carbajo, S.; Doak, R. B.; Ehrenberg, D.; Foucar, L.; Gasper, R.; Gorel, A.; Hilpert, M.; Kloos, M.; Koglin, J. E.; Reinstein, J.; Roome, C. M.; Schlesinger, R.; Seaberg, M.; Shoeman, R. L.; Stricker, M.; Boutet, S.; Haacke, S.; Heberle, J.; Heyne, K.; Domratcheva, T.; Barends, T. R. M.; Schlichting, I. Three-Dimensional View of Ultrafast Dynamics in Photoexcited Bacteriorhodopsin. *Nat. Commun.* **2019**, *10* (1), 3177.
(37) Taguchi, S.; Niwa, S.; Dao, H.-A.; Tanaka, Y.; Takeda, R.; Fukai, S.; Hasegawa, K.; Takeda, K. Detailed Analysis of Distorted Retinal and Its Interaction with Surrounding Residues in the K Intermediate of Bacteriorhodopsin. *Commun. Biol.* **2023**, *6* (1), 190.
(38) Nogly, P.; Weinert, T.; James, D.; Carbajo, S.; Ozerov, D.; Furrer, A.; Gashi, D.; Borin, V.; Skopintsev, P.; Jaeger, K.; Nass, K.; Båth, P.; Bosman, R.; Koglin, J.; Seaberg, M.; Lane, T.; Kekilli, D.; Brünle, S.; Tanaka, T.; Wu, W.; Milne, C.; White, T.; Barty, A.; Weierstall, U.; Panneels, V.; Nango, E.; Iwata, S.; Hunter, M.; Schapiro, I.; Schertler, G.; Neutze, R.; Standfuss, J. Retinal Isomerization in Bacteriorhodopsin Captured by a Femtosecond X-Ray Laser. *Science* **2018**, *361* (6398), eaat0094.
(39) Borshchevskiy, V.; Kovalev, K.; Round, E.; Efremov, R.; Astashkin, R.; Bourenkov, G.; Bratanov, D.; Balandin, T.; Chizhov, I.; Baeken, C.; Gushchin, I.; Kuzmin, A.; Alekseev, A.; Rogachev, A.; Willbold, D.; Engelhard, M.; Bamberg, E.; Büldt, G.; Gordeliy, V. True-Atomic-Resolution Insights into the Structure and Functional Role of Linear Chains and Low-Barrier Hydrogen Bonds in Proteins. *Nat. Struct. Mol. Biol.* **2022**, *29* (5), 440−450.
(40) Matsui, Y.; Sakai, K.; Murakami, M.; Shiro, Y.; Adachi, S.; Okumura, H.; Kouyama, T. Specific Damage Induced by X-Ray Radiation and Structural Changes in the Primary Photoreaction of Bacteriorhodopsin. *J. Mol. Biol.* **2002**, *324* (3), 469−481.
(41) Lanyi, J. K. Molecular Mechanism of Ion Transport in Bacteriorhodopsin: Insights from Crystallographic, Spectroscopic, Kinetic, and Mutational Studies. *J. Phys. Chem. B* **2000**, *104* (48), 11441−11448.
(42) Cooper, A. Energy Uptake in the First Step of Visual Excitation. *Nature* **1979**, *282* (5738), 531−533.
(43) Schick, G. A.; Cooper, T. M.; Holloway, R. A.; Murray, L. P.; Birge, R. R. Energy Storage in the Primary Photochemical Events of Rhodopsin and Isorhodopsin. *Biochemistry* **1987**, *26* (9), 2556−2562.
(44) Gascon, J. A.; Batista, V. S. QM/MM Study of Energy Storage and Molecular Rearrangements Due to the Primary Event in Vision. *Biophys. J.* **2004**, *87* (5), 2931−2941.
(45) Tsujimura, M.; Chiba, Y.; Saito, K.; Ishikita, H. Proton Transfer and Conformational Changes along the Hydrogen Bond Network in Heliorhodopsin. *Commun. Biol.* **2022**, *5* (1), 1336.
(46) Albeck, A.; Livnah, N.; Gottlieb, H.; Sheves, M. Carbon-13 NMR Studies of Model Compounds for Bacteriorhodopsin: Factors Affecting the Retinal Chromophore Chemical Shifts and Absorption Maximum. *J. Am. Chem. Soc.* **1992**, *114* (7), 2400−2411.
(47) Mak-Jurkauskas, M. L.; Bajaj, V. S.; Hornstein, M. K.; Belenky, M.; Griffin, R. G.; Herzfeld, J. Energy Transformations Early in the Bacteriorhodopsin Photocycle Revealed by DNP-Enhanced Solid-State NMR. *Proc. Natl. Acad. Sci. U.S.A.* **2008**, *105* (3), 883−888.

https://doi.org/10.1021/acs.jpcb.4c00804
J. Phys. Chem. B 2024, 128, 5966−5972